

Definition 1: Reynolds Number Re

Compares advection of momentum to frictional acceleration.

$$Re = \frac{UL}{\nu}$$

Definition 2: Rossby Number Ro

Compares advection of momentum to Coriolis acceleration.

$$Ro = \frac{U}{fL}$$

Definition 3: Rhines Number R_*

Ratio of Rhines scale to horizontal scale.

$$R_* = \frac{U}{L^2} = \frac{\alpha}{L} Ro$$

Definition 4: Burger Number Bu

Ratio of relative vorticity to *stretching* vorticity.

$$\sqrt{Bu} = \frac{NH}{fL} = \frac{L_R}{L}$$

Definition 5: mass mkg **Definition 6: gravitational acceleration g m/s²**

Value of surface normal component of all body forces.

Definition 7: vorticity ω_1/s **Definition 8: Buoyancy Vector B_1/s^2**

$$\mathbf{B} = -\frac{\nabla \rho \times \nabla p}{\rho^2}$$

Definition 9: Kinetic Energy per mass $E_k m^2/s^2$ **Definition 10: Mechanical Energy per mass $E_k m^2/s^2$**

Sum of kinetic and potential Energy.

Definition 11: Rossby Radius $L_R m$

The *geostrophic wavelength*. $L_R = c/f$

Definition 12: Steering Level z_S

The critical depth where the real part of the Doppler shifted phase speed $c_S(z_S) = c(z) - u(z) = 0$ vanishes. I.e. the depth where the Doppler shift creates a standing wave, causing the disturbances to grow in place instead of spreading in space, analogous to a *supersonic bang*.

Definition 13: Rhines Scale L_r [m]

Scale at which earth's sphericity becomes important.

$$L_r^2 = \frac{U}{\beta} \quad (1)$$

Assuming Gaussian shape:

$$h = A e^{-(x/\sigma)^2/2}$$

$$\text{with } A = a' + a = A e^{-1/2} + a$$

$$\begin{aligned} \frac{\partial h(\sigma)}{\partial x} &= -\frac{A}{\sigma} e^{-1/2} \\ &= -\frac{a'}{\sigma} \end{aligned}$$

hence

$$\begin{aligned} L_r &= \sqrt{\frac{g}{f} \frac{\partial h}{\partial x} \beta} \\ L_r &= \sqrt{\frac{ga'}{f\sigma\beta}} \end{aligned} \quad (2)$$

TODO:en detail:

$$\begin{aligned} \frac{\partial h(\sigma)}{\partial x} &= -\frac{A}{\sigma} e^{-1/2} \\ &= -\frac{a}{\sigma} \frac{e^{-1/2}}{(1 - e^{-1/2})} \\ &= \frac{a}{\sigma (e^{1/2} - 1)} \end{aligned}$$

hence

$$\begin{aligned} L_r &= \sqrt{\frac{g}{f} \frac{\partial h}{\partial x} \beta} \\ L_r &= \sqrt{\frac{g}{e^{1/2} - 1} \frac{a}{f\sigma\beta}} \end{aligned} \quad (3)$$

Definition 14: Gravity Wave Phase Speed c cm/s

$$c = \sqrt{g'H}$$

Definition 15: Reduced Gravity $g'(x, y, z) m/s^2$

$$\text{In the layered model } g' = g \frac{\delta\rho}{\rho_0} = N^2 h$$

Definition 16: Surface/interface Displacement $\eta(x, y) m$ **Definition 17: Brunt Väisälä frequency N_1/s**

$$N^2 = g/\rho_0 \frac{\partial \rho}{\partial z}$$

Definition 18: Mean Layer thickness H_m **Definition 19: Layer Thickness/physical height of an isopycnal surface $h(x, y, t) m / h(x, y, \rho, t) m$**

$$h = H + \eta \text{ (in the layered model)}$$

Definition 20: Planetary Vorticity Ω_1/s

$$\Omega = 4\pi/\text{day}_{fix\star}$$

Definition 21: Latitude ϕ_{rad}

Definition 22: Earth's Radius a_m **Definition 23: Surface-Normal Planetary Vorticity Component $f_{1/s}$**

$$f = \cancel{f} z = \Omega \sin \phi z$$

Definition 24: Change of Planetary Vorticity with Latitude $\zeta \text{ 1/ms}$

$$\zeta = \frac{\partial f}{\partial y} = \Omega/a \cos \phi$$

Definition 25: Okubo-Weiss Parameter $O_w \text{ 1/s}^2$

$O_w = \text{divergence}^2 + \text{stretching}^2 + \text{shear}^2 - \text{vorticity}^2$.

A negative value indicates vorticity dominated motion, whereas a positive value indicates deformation.

Definition 26: Sea Surface Height SSH m **Definition 27: Isoperimetric Quotient IQ**

$$IQ = A/A_c = \frac{A}{\pi r_c^2} = \frac{4\pi A}{U^2} \leq 1.$$

The ratio of a ring's area to the area of a circle with equal circumference.

Definition 28: Gaussian radius r_m

$$(H - a) = H \exp\left(-\frac{A}{2\pi r^2}\right).$$

Twice the Gaussian standard-deviation.

a : amplitude

H : Gaussian amplitude

A : determined area

Definition 29: dynamic eddy scale σ_m

Distance from eddy's center to the line of maximum orbital speed *i.e.* the zero-vorticity contour.

Definition 30: Run **AVISO -MI**

7-day time-step aviso with method **MI**.

Definition 31: Run **AVISO -MII**

7-day time-step aviso with method **MII**.

Definition 32: Run **pop2avi-MII**

7-day time-step POP remapped to aviso-geometry with method **MII**.

Definition 33: Run **POP-7day-MII**

7-day time-step POP with method **MII**.

Definition 34: Run **POP-1day-MII-Southern-Ocean**

1-day time-step aviso with method **MII**.

Southern Ocean Only.

Minimum Age: **TODO:SI**

Contour step raised to **TODO:SI**

Definition 35: Parallel Ocean Program (POP).

Global fully non-linear $o^{\circ}6'$, **TODO:SI** primitive equation ocean model Oestreicher [22].

Definition 36: AVISO

Merged ERS-1/Topex-data Forget [14].

Definition 37: Anti-cyclone (AC)

A vortex with sign of rotational vector opposite to Ω .

Definition 38: Cyclone (C)

A vortex with sign of rotational vector equal to Ω .

THE MAIN PURPOSE of this study is to create a computer program that is able to **detect**, **track** and **analyse** meso-scale ocean eddies via their surface signal in sea-surface-height (SSH). Due to the inherently technical character of the matter, large parts are dedicated to technicalities of the algorithm¹. Oceanographic results are treated in the **results**- and **discussion**-chapters. This chapter discusses the physics of meso-scale geostrophic turbulence and introduces a handful of relevant historical papers. Since focus is on horizontal scales, translational speeds and the comparison of results between the **AVISO** -altimetry product and SSH-data from the **POP** ocean model, sections generally focus on either of these three topics.

¹ see the methods-??.

0.1 Theory

THIS section discusses the theory of meso-scale turbulence and parametrizations thereof. Geostrophic turbulence is typically characterized by rather stable, circular, coherent pressure anomalies, that rotate fluid around in a vortex in quasi-geostrophic equilibrium. These entities can persist for long periods of time in which they often travel distances on the order of hundreds of kilometers zonally. The fact that baroclinic instability leads to these vortices, instead of cascading to ever smaller scales as would be expected from chaotic turbulence, is a direct consequence of the inverse energy cascade of two-dimensional motion² (see ??.). The atmospheric analog are

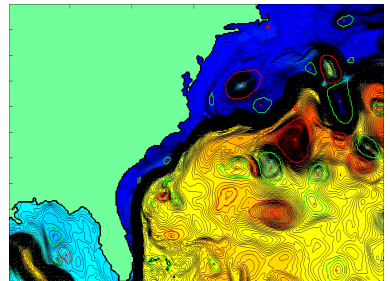


Figure 1: Animation snapshot of early test run. Shown is SSH with detected eddies indicated by red and green lines.

² For a discussion of this phenomenon see ??

storms and high-pressure systems, yet with much less difference between high- and low-pressure systems due to a smaller centrifugal force *i.e.* smaller Rossby number (Ro). These quasi-geostrophic, meso-scale vortices, from here on called eddies³, are immediately visible on SSH-maps (see fig. 3). Yet, it is difficult to physically *define* an eddy in terms of oceanographic variables. The transition from meandering jets or other undeveloped baroclinic turbulence to a coherent vortex is not very sharp. Eddies also sometimes merge or split or collectively form rifts and valleys in SSH. Detecting them on one snapshot automatically via an algorithm is therefore not trivial. Further problems arise when the algorithm is also supposed to track each individual over time. Their sheer abundance at any given time inevitably creates ambiguities as to *which is which* between time steps.

TODO:do O_w over!

0.1.1 Detection methods

- One way to find an eddy in SSH-data is to simply scan for closed contours at different values for z and then subject found entities to a series of geometric tests. Only if all criteria are met is an eddy found. This method was first used by Chelton *et al.* [4] and is certainly a relatively simple yet very effective method, at least so for satellite data. Therefore, as a starting point, this method will be adopted and should also serve as a general definition of what will be referred to as an *eddy* hereafter⁴.

Chelton *et al.* set the following threshold criteria for his algorithm:

1. The SSH values of all of the pixels are above (below) a given SSH threshold for anticyclonic (cyclonic) eddies.
2. There are at least $[threshold]$ pixels and fewer than $[threshold]$ pixels comprising the connected region.
3. There is at least one local maximum (minimum) of SSH for anticyclonic (cyclonic) eddies.
4. The amplitude of the eddy is at least $[threshold]$.
5. The distance between any pair of points within the connected region must be less than $[threshold]$.

³For a discussion of the different types of vortices in the ocean see appendix ??

⁴The vortices will have names deviant from *eddy* where these criteria are altered.

- Another frequently used method to define an eddy makes use of the strain tensor ⁵ \mathbf{T} . The trace of the strain tensor squared includes valuable information about the dynamics of the velocity field. Namely

⁵ see Derivation ??

$$2\mathcal{O}_W = \text{Tr } \mathbf{T}^2 = \text{divergence}^2 + \text{stretching}^2 + \text{shear}^2 - \text{vorticity}^2 \quad (4)$$

which reduces to $\mathcal{O}_W = (\partial_x u)^2 + 2\partial_y u \partial_x v$ in two dimensions. This is called the Okubo-Weiss-Parameter [23]. It is a useful tool to determine whether the field has parabolic, vorticity dominated character, or whether deformation dominates, giving hyperbolic character. An area of large negative values indicates high enstrophy density compared to gradients of kinetic energy, thus indicating little friction paired with high momentum *i.e.* a coherent, angular-momentum-conserving entity. Positive values on the other hand indicate incoherent deformation.

As ingenious as this parameter seems, it turns out that using it to identify eddies is often not the best solution. Chelton *et al.* [4] name 3 major drawbacks:

- *No single threshold value for \mathcal{O}_W is optimal for the entire World Ocean. Setting the threshold too high can result in failure to identify small eddies, while a threshold that is too low can lead to a definition of eddies with unrealistically large areas that may encompass multiple vortices, sometimes with opposite polarities.*
- \mathcal{O}_W is highly susceptible to noise in the SSH field. Especially when velocities are calculated from geostrophy, the sea surface has effectively been differentiated twice and then squared, exacerbating small discontinuities in the data.
- *The third problem with the W-based method is that the interiors of eddies defined by closed contours of W do not generally coincide with closed contours of SSH. The misregistration of the two fields is often quite substantial.*

It is hence only logical to scan for closed contours of SSH directly (as was done so by Chelton *et al.*).

0.1.2 Eddy Drift Speeds

Intuitively any translative motion of a vortex should stem from an asymmetry of forces as in an imperfectly balanced gyroscope wobbling around and translating across a table. The main effects that cause a quasi-geostrophic ocean eddy to translate laterally can rel. easily be explained heuristically.

TODO:equations to follow Cushman-Roisin [6] van Leeuwen [30]

Drift Speed 1 - Lateral Density Gradient

Consider a mean layer-thickness gradient $\frac{\partial h}{\partial x} > 0$ somewhere in the high northern latitudes and a geostrophic, positive density anomaly within that layer. In other words, a high-pressure vortex or an anti-cyclonic eddy with length scale $L \approx L_R$. Next consider a parcel of water adjacent to the eddy's northern flank of initially zero relative vorticity that is being entrained by the eddy. As the clockwise rotating eddy advects the parcel towards its eastern side, the water-column comprising said fluid will be stretched vertically as it is advected towards larger depths. In order to maintain total vorticity a small new relative-vorticity term is introduced via term C in equation (??). Since the vorticity budget is dominated by the planetary component, this new term has sign of f i.e. **positive**. The opposite effect holds for a parcel advected towards the western side. Then, vortex *squeezing* leads to a new **negative** relative-vorticity term. Hence water masses on both sides of the thickness gradient acquire rotation that slowly pushes the eddy in the direction $-f \times \frac{\partial h}{\partial x}$ (in this case south). Note that since vorticity is dominated by the planetary component, the rotational sense of the eddy is irrelevant here. I.e. water columns stretched [squeezed], will always lead to new ω with sign of f [$-f$].

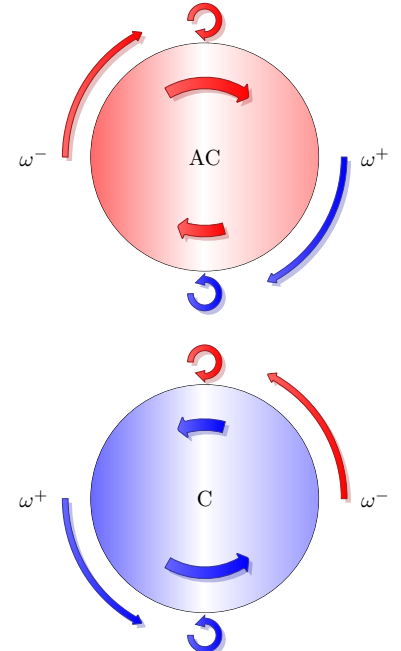


Figure 2: Bottom [Top]: Northern hemisphere [anti]cyclone. Blue [red] color indicates presence/production of positive [negative] relative vorticity. Advection of adjacent water masses leads to a westward drift, irrespective of the eddy's sign (see box 2). Inside, the discrepancy in swirl strength between north and south requires another (smaller) zonal drift term, which is eastward [westward] for [anti]cyclones.

Drift Speed 2 - Planetary Lift

Assume now that L be comparable or larger even than $f + \omega$ from the previous example. Then, independent of layer-thickness, all fluid adjacent to the eddy on its northern and southern flanks will be transported meridionally, thereby be tilted with respect to Ω and hence acquire relative vorticity to compensate. All fluid transported north [south] will balance the increase in planetary vorticity with a decrease [increase] in relative vorticity. This is again independent of the eddy's sense and in this case also independent of hemisphere since $\frac{\partial f}{\partial y} = 0 > 0$ for all latitudes. The result is that small negative vortices to the northern and small positive vortices to the southern flank of eddies will push them west.

Drift Speed 3 - Eddy-Internal -Effect

In the later case clearly particles within the vortex undergo a change in planetary vorticity as well. Or from a different point of view, since $U \sim \nabla p / f$, and noting that the pressure gradient is the driving force here and hence fix at first approximation, particles drifting north will decelerate and those drifting south will accelerate. In order to maintain mass continuity, the center of volume will be shifted west for an anti-cyclone and east for a cyclone. Another way to look at it is to note that the only way for the discrepancy in Coriolis acceleration north and south, whilst maintaining constant eddy-relative particle speed, is to superimpose a zonal drift velocity so that net particle velocities achieve symmetric Coriolis acceleration.

0.1.3 The Integral Length Scale of Turbulence

THISsection discusses the motivation for exact determinations of *eddy scales*. That is, their horizontal extent *i.e.* their diameter or *wavelength*.

JUSTlike the eddy itself, its scale is rather vague and difficult to define. What physical parameter defines the outer edge of a seamless, smooth vortex? If the eddy is detected as done by Chelton *et al.* [4], *i.e.* closed contours of SSH, the interior of which fulfilling certain criteria, the measured perimeter may jump considerably from one time step to the next. An incremental difference in the choice of z might translate to a perimeter outlining twice the difference in area, especially when SSH gradients are small.

Another possibility is to define an amplitude first, then assume a certain shape *e.g.* Gaussian, and then infer the radius indirectly. The obvious problem with this approach would be to properly define the amplitude.

The most physically sound method would have to be one depending on the eddy's most defining physical variable that is unambiguously determinable from SSH: the geostrophic velocities. Chelton *et al.* [4], as with everything else, tried all methods but also conclude that the later is the most adequate one⁶.

⁶ See Chapter ??

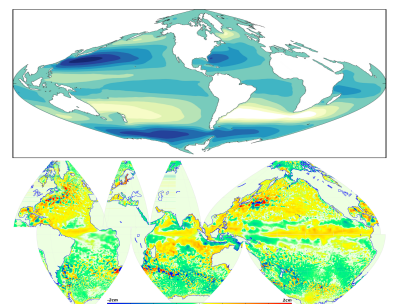


Figure 3: top: Stommel's equation $F_{\text{bottom}} - F_{\text{surface}} = -V\beta$ with constant eddy viscosity. bottom: POP eddy-resolving model snapshot with SSH mean of one year subtracted.

CONSTRUED as an integral length scale of turbulence *i.e.* as the distance at which the auto-correlation of particles reaches zero, the *eddy-scale* turns out to be of fundamental relevance for attempts to parametrize geostrophic turbulence.

General circulation models ($\Theta(10^2)$ km) as they are used in *e.g.* climate forecasts are too coarse to resolve meso-scale ($\Theta(10^1)$ km) turbulence [16, 11, 10, 7, 8, 29, 12, 9, 2, 15]. Even if the Von-Neumann-condition were ignored and a refinement were desired horizontally only, a leap of one order of magnitude would effect an increase in calculation time⁷ of factor $x = 100$. The effects of the nonlinear terms therefore have to be somehow articulated in an integral sense for the large grid-boxes in the model. A common approach is to assume that *eddy kinetic energy* $\bar{u}'\bar{u}'$ and *eddy potential energy* $\bar{w}'\bar{\rho}'$, akin to diffusive processes⁸, were proportional to the gradient of \bar{u} respective \bar{b} (down-gradient-parametrization⁹) Olbers *et al.* [24], which leads to the problem of finding expressions for the *turbulent diffusivities* *i.e.* the rate at which gradients are diffused by turbulence. This parameter is by no means constant, instead it can span several orders of magnitude, itself depending on the strength of turbulence-relevant gradients, and sometimes even assuming negative values Eden & Greatbatch [10]. Precise knowledge of the integral length scale and the physics that set it is hence vital for attempts to analyze and set values for eddy diffusivities and turbulence parametrizations in general.

TODO:[...] i took out section on eddy diffusivities

0.2 Important Papers

THE following discusses a handful of selected historical papers that are concerned with either the theory of mesoscale eddies or with the detection/tracking of eddies from SSH data.

0.2.1 Waves and Turbulence on a β -Plane¹⁰

Rhines investigated the effect of the β -plane on the inverse energy cascade of quasi-2-dimensional atmospheric and oceanic turbulence. At constant f , energy should be cascaded to ever-larger scales until halted by the scale of the domain. This is

⁷ With the Moore's-Law-type exponential growth in FLOP/S of the last 22 years for supercomputers ($\lg(x) \sim 3/11a$) a factor 100 interestingly translates to only $a = 22/3 \approx 7$ years...

⁸ In analogy to Fick's first law of diffusion.

⁹ *i.e.* Reynolds averaging

¹⁰ Rhines, Peter B. 1974. Waves and turbulence on a beta-plane. *J. Fluid Mech.*, **69**(03), 417

clearly not the case, as no storm has ever grown to global scale. The presence of a meridional restoring force creates a critical scale beyond which the *turbulent migration of the dominant scale nearly ceases* Rossby waves are excited which would in theory eventually give way to alternating zonal jets of width L_c . This scale was later coined the Rhines Scale L_c .

0.2.2 Westward Motion of Mesoscale Eddies¹¹

Bjerknes & Holmboe [1] already noted that the ζ -effect causes a mass-imbalance in planetary vortices that, if not met by an asymmetry in shape must lead to westward propagation.

Nof [21] derived that the ζ -effect results in a net meridional force on the integrated mass of the vortex, which in balance with the Coriolis acceleration shoves cyclones eastward and anti-cyclones westward. They also explained how displaced water outside the eddy's perimeter causes a much stronger westward component, with the result that all eddies propagate westward irrespective of rotational sense.

The westward drift was also derived in various forms by e.g. Flierl [13], Matsuura & Yamagata [20].

THE paper by Cushman-Roisin [6] is particularly helpful to understand where the two components of westward drift come from. By scaling the terms in the one-layer primitive equations by their respective dimensionless numbers, integrating the interface-displacement caused by the eddy over the eddy's domain and applying mass continuity they derive for the location (X, Y) of an eddy's centroid¹²:

$$\begin{aligned} \Pi X_{tt} - Y_t &= L_R T \beta \langle yv \rangle + L \frac{\beta}{f} \langle y\eta v \rangle \\ \Pi Y_{tt} - X_t &= -L_R T \beta \langle yu \rangle - L \frac{\beta}{f} \langle y\eta u \rangle \end{aligned} \quad (5)$$

where $\Pi = 1/f_0 T$.

Hence, independent of balance of forces the eddy's center of mass describes inertial oscillations¹³ on the f-plane, even in the absence of ζ . Using geostrophic values for u and returning

¹¹ Cushman-Roisin, B. 1990. Westward motion of mesoscale eddies. *J. Phys.* ...

¹² $\langle \rangle \equiv \frac{1}{A} \int_A dA$

¹³ compare to harmonic oscillator

to dimensional variables equation (5) can be cast into:

$$\frac{\partial X}{\partial t} = \frac{\beta g' \int_A H\eta dA + \int_A \eta^2/2 dA}{f_o^2} \quad (6)$$

$$= \beta \left(\frac{NH}{f_o} \right)^2 \left(1 + \frac{1}{H} \frac{\int \eta^2 dA}{2V_e} \right) \quad (7)$$

$$= \frac{\partial \omega_{long}}{\partial k} \left(1 + \frac{1}{H} \frac{\int \eta^2 dA}{2V_e} \right) \quad (8)$$

TODO:make better

The first term of the RHS of eq. (7) represents the *planetary lift*¹⁴, which is identical to the zonal group velocity of long Rossby waves [?]. The second term represents the *eddy internal -effect* (see box 3). Note that the first term is always westwards, while the second has sign of $-\eta$, i.e. westward for anti-cyclones and eastward for cyclones and that the first is always larger than the second.

¹⁴ see box 2 from section 0.1.2

TODO:van Leeuwen [30] for derivation if time

0.2.3 Early Altimeter Data

THE advent of satellite altimetry, which Walter Munk called *the most successful ocean experiment of all time* Orbach & Munk [25], finally allowed for global-scale experimental investigations of oceanic planetary phenomena on long time- and spatial scales. Among others, Matano *et al.* [19], Cipollini *et al.* [5], Le Traon & Minster [18] were the first to use satellite-data to present evidence for the existence of Rossby waves and their westward-migration in accord with theory. Surprisingly all of the observations found the phase speeds to be 1 to 1.5 times larger than what theory predicted. Several theories to explain the discrepancy were presented. E.g. Killworth *et al.* [17] argued that the discrepancy was caused by mode-2-east-west-mean-flow velocities. Interestingly it appears that hitherto, the relevant altimeter signal was mainly associated with linear waves. Non-linearities are rarely mentioned in the papers of those years. Probably simply due to the fact that the turbulent character of much of the meso-scale variability was still obscured by the poor resolution of the first altimeter products.

0.2.4 SSH Altimeter Data¹⁵

From the beginning of satellite altimetry Chelton *et al.* have invested tremendous effort to thoroughly analyze the data in terms of Rossby waves and geostrophic turbulence. At the time of the Killworth *et al.* [17] paper only 3 years of Topex/Poseidon data alone had been available, which led them to interpret the data mainly in terms of Rossby waves. Once the merged Aviso T/P and ERS 1/2 Forget [14] was released 7 years later, Chelton *et al.* presented a new analysis that was based on an automated eddy-tracking algorithm using the geostrophic Okubo-Weiss parameter^{16,17}. For the first time satellite data was resolved sufficiently fine to unveil the dominance of *blobby structures rather than latitudinally refracted continuous crests and troughs* that had hitherto been assumed to characterize the large-scale SSH topography. They presented results of a refined algorithm in their 2011 paper, in which they abandoned the Okubo-Weiss concept and instead identified eddies via closed contours of SSH itself¹⁸. The improved algorithm and longer data record now allow them to separate the non-linear eddy-activity from the larger-scale Rossby waves. They find that the vast majority of extra-tropical westward propagating SSH-variability does indeed consist of coherent, isolated, non-linear, mesoscale eddies that propagate about 25% slower¹⁹ than the linear waves. Apart from this they find little evidence for any dispersion in the signal, neither do they find evidence for significant meridional propagation, as should be found for Rossby waves. In agreement with Rhines & Holland [27], they find this eddy-dominated regime to fade towards the equator, giving way to the characteristic Rossby wave profile. Almost all of their eddies propagate westwards. Those eddies that are advected eastwards by *e.g.* the ACC show significantly shorter life-times than those that are not. For more detail on their results and a discussion of the limitations of eddy-tracking via satellites see section ??.

¹⁵ Chelton, Dudley B., Schlax, Michael G., Samelson, Roger M., & de Szoeke, Roland a. 2007. Global observations of large oceanic eddies. *Geophys. Res. Lett.*, **34**(15), L15606; and Chelton, Dudley B., Schlax, Michael G., & Samelson, Roger M. 2011. Global observations of nonlinear mesoscale eddies. *Prog. Oceanogr.*, **91**(2), 167–216

¹⁶ see section 0.1.1

¹⁷ see Derivation ??

¹⁸ note that geostrophic O_W is a second derivative of SSH and thus exacerbates noise in the SSH data.

¹⁹ pointing to dispersion.

0.3 Methods

0.3.1 Satellite- vs Model Data

The latest AVISO SSH data from satellites features impressive accuracy, constancy and resolutions in both space and time. This is achieved by collecting all of the data from all of the altimeter-equipped satellites available at any given moment for any given coordinate. This conglomerate of highly inhomogeneous data is then subjected to state-of-the-art interpolation methods to produce a spatially and temporally coherent product. One satellite alone is not sufficient to adequately resolve meso-scale variability globally.

E.g. the Topex/Poseidon satellite had a ground repeat track orbit of 10 days and circled the earth in 112 minutes or ≈ 13 times a day with a swath width of 5 km. Hence it drew ~ 26 5-km-wide stripes onto the globe every day. This pattern is then repeated after 10 days, which means that at the equator only $10 \times 26 \times 5 = 1300$ km of the $2\pi \times 6371 = 40000$ km get covered, *i.e.* 3.25%. At every 10d time-step, on average, effectively $40000/1300 - 5 = 20$ km are left blank in-between swaths on the equator. This is why, no matter how fine the resolution within the swath at one moment in time may be, the spatial resolution is so coarse.

THE merged ERS-1/Topex-data as used by Chelton *et al.* [4] has a time step of 7 days. Assuming eddy drift speeds of $u_e = 0 (10^{-1})$ m/s implies a distance traveled per time step of $L_{\delta t} \approx 60$ km. Chelton *et al.* estimate their effective spatial resolution as $\delta x \approx 40$ km. Eddies of smaller scale are not resolved.

TRACKING a single eddy from one time-step to the next is complicated by the sheer abundance of eddies at any given point in time and the fact that eddy activity is usually concentrated into regions of strong geostrophic turbulence.

THE ambiguities in matching the eddies from the old time-step to those of the new one might cause aliasing effects in the final statistics.

THE translational speeds ²⁰ of eddies are not really the prob-

	POP	merged T/P - ERS-1
$\frac{\delta x}{\delta t}$	7km 11km	$\frac{1}{3}$ ≈ 40 km (≈ 40 km after filtering)
dt	1d	7d
$\log_{10} 2$ filter cutoff	n/a	2° by 2°
z-levels	42	1
variables	SSH, S, T, u/v/w,	SSH

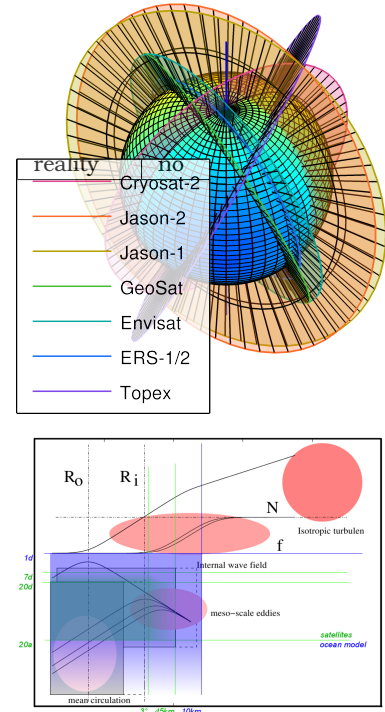


Figure 4: Resolutions for model vs satellite. Modified version from Olbers *et al.* [24].

²⁰ $O (10^1)$ km/day

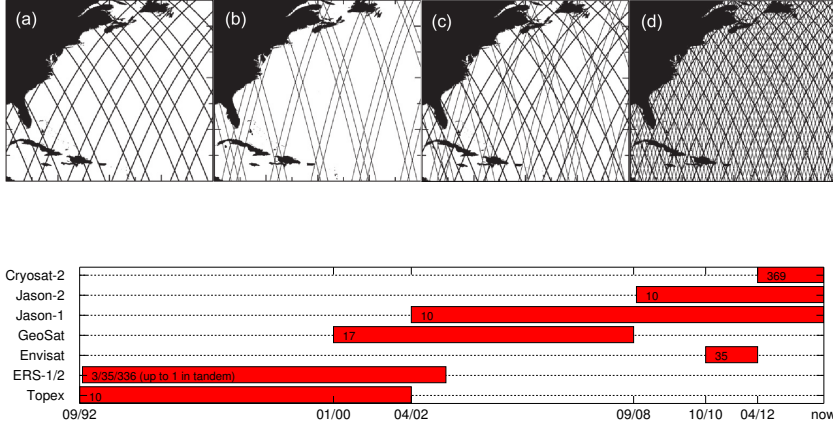


Figure 5: The ground track patterns for the 10-day repeat orbit of T/P and its successors Jason-1 and Jason-2 (thick lines) and the 35-day repeat orbit of ERS-1 and its successors ERS-2 and Envisat (thin lines). (a) The ground tracks of the 10-day orbit during a representative 7-day period; (b) The ground tracks of the 35-day orbit during a 7-day period (performed today); (c) The ground tracks of the 10-day orbit and the 35-day orbit during the 7-day period; and (d) The combined ground tracks of the 10-day orbit and the 35-day orbit during the full 35 days of the 35-day orbit. (sic) Chelton *et al.* [4]

lem here, as they usually drift slow enough to not cover more than 1 grid node per 7 day time step. The issue are those areas where eddies are born, die and merge. According to Smith & Marshall [28], instabilities within the ACC grow at rates of up to $1/(2\text{days})$, which means that at one time-step up to 3 eddies have emerged and equally many died for every eddy identified within such region. The ground-repeat-frequency of a satellite can of course not be set arbitrarily. Especially when the satellite is desired to cover as far north and south as possible, whilst still being subjected to just the right torque from the earth's variable gravitational field to precess at preferably a sun-synchronous frequency *i.e.* $360^\circ/\text{year}$?]. Neither can the satellite's altitude be chosen arbitrarily. If too low the oblateness of the earth creates too much eccentricity in the orbit that can no longer be *frozen*²¹. Another problem could be potential inhomogeneity in the merged data in time dimension, since data of old and current missions are lumped together into one product. This is why Chelton *et al.* [4] opted against the finest resolution available and instead went for a product that had the most satellites merged in unison for the longest period of time.

Box 1 - Horizontal Resolution

Assume $Bu = 1$, so that $L = NH/f$ and $NH = \alpha/10d$ (corresponds to $L(\phi = 30^\circ) = 100\text{km}$), a model resolution of $1^\circ/\mu$ and that the eddy diameter was twice the Rossby

²¹ minimizing undulating signals in altitude by choosing the right initial values ?]

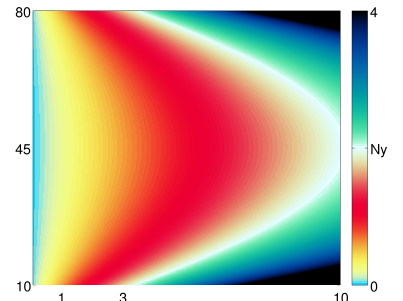


Figure 7: $\xi(\phi, \mu)$. $Ny \equiv 2$ *i.e.* the Nyquist frequency.

radius. Then, how many grid nodes ξ fit into one eddy as a function of latitude?

$$\begin{aligned} \xi \frac{a \cos \phi}{2\pi} &= \frac{2NH}{f} = \frac{2NH_1 d}{4\pi \sin(\phi)} \\ \xi &= \frac{2\mu}{10 \sin(2\phi)} \end{aligned} \quad (9)$$

In this flat-bottom, constant ρ_z , Mercator-gridded model the worst eddy-resolution is interestingly at mid-latitude (see fig. 7).

THE surface velocities inferred from altimetry are the geostrophic components only, which should suffice to *e.g.* determine the non-linearity and kinetic energy of an eddy for almost all regions, but less so for *e.g.* the western boundary currents. After all though, one must keep in mind that by using model data, what one analyses is of course just that - a *model*.

0.4 Lengths of Tracks

THE MOST APPARENT DIFFERENCE between the results of the [two detection-methods](#) is the abundance of long-lived eddies resulting from the [MI](#)-method. This discrepancy must logically be caused by the two different contour-shape-testing procedures ([????](#)), since it is here where the main difference between the two methods' algorithms lies.

THE [MI](#)-method is the more lenient one, as all it checks for, is whether the contour is of sufficiently compact form. The only shapes that are dismissed are long, thin elongated structures. This means that *e.g.* an eddy track can more easily ²² survive situations in which two eddies merge into one or those in which one is split into two or situations in which mean current gradients distort the vortex.

There could also be the situation in which an old, weak eddy fades, yet another one emerges in sufficient proximity. These two events would not even have to coincide at the exact same time, as long as some short-lived coherent structure, of which there is an abundance ²³ at any given time-step throughout the world ocean, acted as a *bridge* to fill the gap.

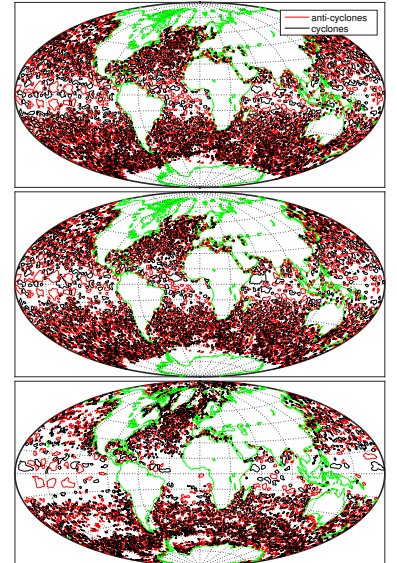


Figure 8: All contours that passed the filtering procedure for one exemplary time-step. Top: [AVISO - MI](#). Mid: [AVISO - MII](#). Bottom: [POP-7day-MII](#).

²² as long as the similarity-criterion is not violated.

²³ see ??

THE **MII** -method is conceptually different in that it is based on the assumption that a distinct coherent vortex need *per definition* to be more or less circular. It will therefore be more likely to regard *e.g.* the situation in which one eddy merges with another as a situation of 3 eddies in total; **two** that have just died to create **one** new one. The focus here is more on the propagation of distinct circular geostrophic vortices whereas the focus in the **MI** -method is more general on coherent local depressions respective elevations in SSH. Unfortunately the time-frame of this work did not allow to test to which degree tracers²⁴ found within tracked eddies remained within the eddy over time. This could further clarify the assumption that the **MI** -method may be better at tracking water-mass advecting entities, with less jumps between bodies of water within one track.

0.5 Scales

INTERESTINGLY , even in the **AVISO -MI** results, the horizontal eddy scale σ differs from that presented by Chelton *et al.* [4]. For latitudes $\gtrsim |25^\circ|$ the zonal mean here is smaller than theirs while for low latitudes it is higher (see ??). The reason for this discrepancy is suspected to stem from the special method by which σ is determined by our algorithm. As outlined in ??, here σ is half the mean of zonal and meridional distances between the first two local extrema of the first derivative of interpolated 4th-order fourier fits to the SSH data around the eddy's CoV . The motivation to use fits instead of the SSH directly was on the one hand to avoid noise complicating correct determinations of the 2nd differential zero-crossings and on the other hand to tackle the problem of coarse resolution, especially so for high latitudes where σ seems to become as small as only twice the distance between data points. At this resolution the Gaussian RMS width of an eddy would amount to only 5 data points. Since σ is generally smaller in the higher-resolution

POP-data analyses, we hypothesize that the scales by Chelton *et al.* are biased high for high latitudes. Question remains to what degree this bias is inherent to the **AVISO** product *i.e.* as a smearing effect from the interpolation of multiple coarse

²⁴ in the model data.

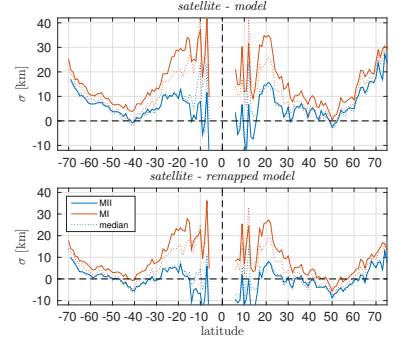


Figure 9: Differences in zonal mean σ between **AVISO** /POP and **AVISO** /downsampled POP . Means/Medians are built zonally over only those $1^\circ \times 1^\circ$ -bins that feature data in both sets *i.e.* the intersection of $\text{lat} + \text{lon}$ of both sets.

satellite data. Or whether it is attributable entirely to the particular method by which the diameter/area of the zero-vorticity contour is estimated.

WITH REGARD to the lower latitudes two important aspects need to be considered:

1. The analyses yield generally low eddy activity in the tropics. Hence the results are less robust in this region *a priori*.
2. The standard deviation in σ is particularly broad in the tropics (see fig. 10). As a matter of fact it appears as though there might be two different types of eddies. One type analogous to all high-latitude eddies and a new one of much larger scale. Because these larger eddies have generally low IQ-values they are filtered from the MII analyses, resulting in smaller tropical σ . Their more chaotic shape might, due to the different methods to determine σ , also have to do with why mean tropical σ is larger here than in Chelton *et al.* [4].

THE POP-7day-MII

analysis yields somewhat similar σ for low latitudes²⁵, yet significantly smaller values for high latitudes. The question therefore is

whether this discrep-

ancy is a result of the lower resolution of the satellite data *i.e.* that eddies are too small to be resolved by the AVISO product in high latitudes or whether it is attributable to the model data as in a systematic bias due to incomplete/poorly parameterised model physics. This question was the primary motivation for the pop2avi-MII -analysis. The idea here was to down-size the POP data to the geometry of the AVISO grid in order to test whether this would raise σ to that from the satellite results. Figure 9 shows that the down-sampling did indeed decrease the discrepancy in σ to respective AVISO analysis, as long as those regions that are unique to either data set are excluded. Between $\pm 25^\circ$ and $\pm 65^\circ$ the difference is no larger than $\pm \text{km}5$. This came as a surprise because since σ stems from fourier fits

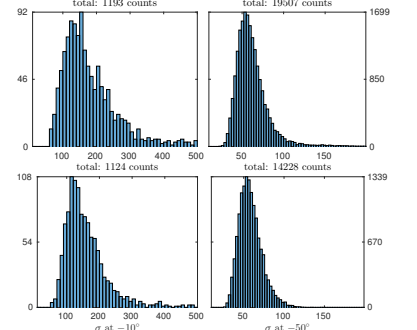


Figure 10: Eddy count at one point in time for one fully zonal 1°-bin. Top: AVISO -MI . Bottom: AVISO -MII . The tropical spectrum is broad yet with strong positive skewness *i.e.* oriented towards smaller scales. In high latitudes the standard deviation is smaller. The MI method yields more large eddies.

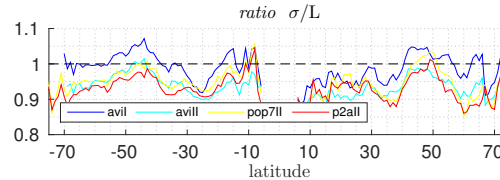


Figure 11: Ratios if σ to L (see ??)

²⁵ Note that due to the lack of tropical eddies the estimates of σ are rather uncertain for the POP analyses.

of SSH, we expected the original frequencies to be, at least to some extent, conserved in the down-sampled data.

THE MI detection method a priori assumes that an eddy is more or less detected at its asymptotic *floor* *i.e.* in the case of an AC at the *foot of the mountain*. The idea of the IQ -based method on the other hand is to assume that the situation of a single well-defined eddy sitting on an otherwise smooth, flat sea surface, which would be necessary for the contour algorithm to find a closed contour describing the outermost perimeter of said single vortex, is unrealistic. Instead the approach is to look for distinct, sufficiently circular caps of SSH-hills/valleys that consistently *wade* through all other weaker geostrophic noise surrounding it. **TODO: why gaussian or quad?**

0.6 Drift Speeds

ZONAL MEAN DRIFT SPEEDS of all AVISO results agree well with those presented by Chelton *et al.* [4] (see ??), suggesting that the tracking procedures are relatively robust for both the MI and MII methods.

THE POP-7day-MII results yield generally smaller magnitudes of u . The apparent drop in magnitude at $\sim 12^\circ\text{N}$ is most likely due to erroneous inter-time-step eddy-associations. In that region, the combination of extreme sparsity of results, large time-step, large σ , low amplitude and high (theoretical) drift speed make robust determinations of u practically impossible. Yet the tendency for lower magnitudes in u , albeit less stark, is also true for higher latitudes. The meridional drift speeds are calculated via gradients of *polyfits* to the CoV -locations on the surface of a spherical earth. This method was tested thoroughly and its robustness is further validated by the fact that the weaker u remains approximately the same after the downsampling for the pop2avi-MII run.

FROM eq. (5) we know that at first approximation (planetary lift)

$$u \sim \beta \left(\frac{NH}{f_0} \right)^2 \quad (10)$$

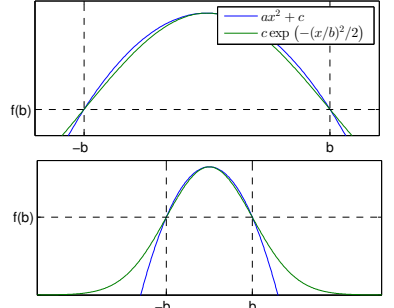


Figure 12: The upper part of a Gaussian profile can appear similar to a quadratic one.

Since β , H and f should be set realistically, it appears that the, apparently unrealisitic, drift speeds in the model results stem from an unrealisitic or poorly resolved (only 42 vertical layers in POP) density stratification $\frac{\partial \rho}{\partial z}$.

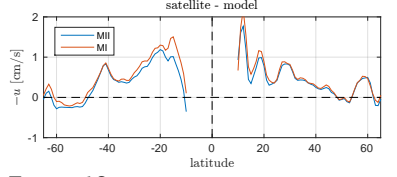


Figure 13: $\text{AVISO -MI} / \text{AVISO -MII}$ minus POP-7day-MII of zonal drift speed means.

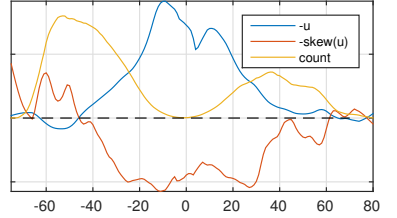


Figure 14: Skewness (red) of $-u$ for AVISO -MI . The spectrum leans towards high westward values in low latitudes. In the ACC the distribution reverses indicating the existence of sporadic events of strong eastward advection by the mean flow. (Note: Everything normalised to fit all in one frame.)

1

Conclusion

TODO:more data, depths, better parallel ...

Bibliography

- [1] Bjerknes, J, & Holmboe, J. 1944. O the Theory of Cyclones. *J. Atmos. Sci.*
- [2] Bryan, K, Dukowicz, JK, & Smith, RD. 1999. On the mixing coefficient in the parameterization of bolus velocity. *J. Phys.* ..., 2442–2456.
- [3] Chelton, Dudley B., Schlax, Michael G., Samelson, Roger M., & de Szoeke, Roland a. 2007. Global observations of large oceanic eddies. *Geophys. Res. Lett.*, **34**(15), L15606.
- [4] Chelton, Dudley B., Schlax, Michael G., & Samelson, Roger M. 2011. Global observations of nonlinear mesoscale eddies. *Prog. Oceanogr.*, **91**(2), 167–216.
- [5] Cipollini, Paolo, Cromwell, David, Jones, Matthew S, Quarterly, Graham D, & Challenor, Peter G. 1997. Concurrent altimeter and infrared observations of Rossby wave propagation near 34 N in the Northeast Atlantic. *Geophys. Res. Lett.*, **24**(8), 889–892.
- [6] Cushman-Roisin, B. 1990. Westward motion of mesoscale eddies. *J. Phys.*
- [7] Eden, Carsten. 2007a. Eddy length scales in the North Atlantic Ocean. *J. Geophys. Res.*, **112**(C6), C06004.
- [8] Eden, Carsten. 2007b. Interpreting eddy fluxes. *J. Phys.* ..., 1–34.
- [9] Eden, Carsten. 2012. Implementing diffusivities from linear stability analysis in a three-dimensional general circulation ocean model. *Ocean Model.*, **57**, 15–28.

- [10] Eden, Carsten, & Greatbatch, Richard J. 2008. Towards a mesoscale eddy closure. *Ocean Model.*, **20**(3), 223–239.
- [11] Eden, Carsten, Greatbatch, Richard J., & Willebrand, Jürgen. 2007. A Diagnosis of Thickness Fluxes in an Eddy-Resolving Model. *J. Phys. Oceanogr.*, **37**(3), 727–742.
- [12] Ferrari, Raffaele, & Nikurashin, Maxim. 2010. Suppression of Eddy Diffusivity across Jets in the Southern Ocean. *J. Phys. Oceanogr.*, **40**(7), 1501–1519.
- [13] Flierl, Glenn R. 1984. Rossby wave radiation from a strongly nonlinear warm eddy. *J. Phys. Oceanogr.*, **14**(1), 47–58.
- [14] Forget, Gaël. 2010. Mapping Ocean Observations in a Dynamical Framework: A 2004–06 Ocean Atlas. *J. Phys. Oceanogr.*, **40**(6), 1201–1221.
- [15] Fox-Kemper, Baylor, Ferrari, Raffaele, & Hallberg, Robert. 2008. Parameterization of Mixed Layer Eddies. Part I: Theory and Diagnosis. *J. Phys. Oceanogr.*, **38**(6), 1145–1165.
- [16] Griffies, SM. 2004. *Fundamentals of ocean climate models*.
- [17] Killworth, Peter D., Chelton, Dudley B., & de Szoeke, Roland A. 1997. The Speed of Observed and Theoretical Long Extratropical Planetary Waves. *J. Phys. Oceanogr.*, **27**(9), 1946–1966.
- [18] Le Traon, P-Y, & Minster, J-F. 1993. Sea level variability and semiannual Rossby waves in the South Atlantic subtropical gyre. *J. Geophys. Res. Ocean.*, **98**(C7), 12315–12326.
- [19] Matano, Ricardo P, Schlax, Michael G, & Chelton, Dudley B. 1993. Seasonal variability in the southwestern Atlantic. *J. Geophys. Res. Ocean.*, **98**(C10), 18027–18035.
- [20] Matsuura, Tomonori, & Yamagata, Toshio. 1982. On the evolution of nonlinear planetary eddies larger than the radius of deformation. *J. Phys. Oceanogr.*, **12**(5), 440–456.
- [21] Nof, Doron. 1981. On the β -induced movement of isolated baroclinic eddies. *J. Phys. Oceanogr.*, **11**(12), 1662–1672.

- [22] Oestreicher, Samantha. Underwater Mathematics : Illuminating Deep-Reaching Ocean Eddies in Climate Models.
- [23] Okubo, Akira. 1970. Horizontal dispersion of floatable particles in the vicinity of velocity singularities such as convergences. *Deep sea Res. Oceanogr. Abstr.*, **17**(143), 445–454.
- [24] Olbers, Dirk, Willebrand, Jürgen, & Eden, Carsten. 2012. *Ocean Dynamics*. Springer.
- [25] Orbach, Michael K, & Munk, Walter. 2002. THE U . S . COMMISSION ON OCEAN POLICY. *Natl. Acad. Sci. Washington, DC*, **15**(April), 135–141.
- [26] Rhines, Peter B. 1974. Waves and turbulence on a beta-plane. *J. Fluid Mech.*, **69**(03), 417.
- [27] Rhines, Peter B, & Holland, William R. 1979. A theoretical discussion of eddy-driven mean flows. *Dyn. Atmos. Ocean.*, **3**(2), 289–325.
- [28] Smith, K. Shafer, & Marshall, John. 2009. Evidence for Enhanced Eddy Mixing at Middepth in the Southern Ocean. *J. Phys. Oceanogr.*, **39**(1), 50–69.
- [29] Treguier, AM. 1997. Parameterization of quasigeostrophic eddies in primitive equation ocean models. *J. Phys.*, 567–580.
- [30] van Leeuwen, Peter Jan. 2007. The Propagation Mechanism of a Vortex on the β Plane. *J. Phys. Oceanogr.*, **37**(9), 2316–2330.